Dynamics of sub-synaptic vesicles and surface microclusters at the immunological synapse

Marco A. Purbhoo[1], Hebin Liu[2], Stephane Oddos[3,4], Dylan M. Owen[4], Mark A. A. Neil[4], Sophie V. Pageon[3], Paul M. W. French[4], Christopher E. Rudd[2], and Daniel M. Davis[3]

[1]Department of Hepatology, Division of Medicine, Medical School Building, Imperial College London, London, W2 1PG, UK

[2]Cell Signaling Section, Division of Immunology, Department of Pathology, Tennis Court Road, University of Cambridge, Cambridge CB2 1QP, UK.

[3]Division of Cell and Molecular Biology, Sir Alexander Fleming Building, Imperial College London, London SW7 2AZ, UK

[4]Department of Physics, Imperial College London, London SW7 2AZ, UK.

Corresponding author:

Daniel M. Davis, Division of Cell and Molecular Biology, Sir Alexander Fleming Building, Imperial College London, South Kensington Campus, London SW7 2AZ, UK.

Tel: +44-207-594-5420; Fax: +44-207-594-3044 E-mail: d.davis@imperial.ac.uk

Word count: 7316

One sentence summary:

Movement of sub-synaptic vesicles rich in LAT is constrained by protein microclusters at T cell immune synapses, dependent on LAT residues important for its binding to SLP-76 and consistent with a role for vesicular LAT in T cell signal transduction.

Abstract

Recent imaging studies have identified clusters of kinases and adaptors that serve as centres of signaling at T cell synapses. Here, we report that ZAP-70, LAT, and SLP-76 accumulated in separate clusters at the interface between T cells and stimulatory anti-CD3 coated coverslips. A fraction of LAT was detected in motile vesicles that repeatedly moved to surface microclusters of SLP-76 where they underwent decreased motility. Moreover, LAT with mutated Y191 and Y226 sites did not dwell at clusters of SLP-76. At intercellular synapses, vesicles containing LAT also co-localized with microclusters of SLP-76, as detected using laser tweezers to orientate T cell/APC conjugates vertically for high-resolution imaging. Phosphorylation of LAT at residues Y191 and Y226 was most prominent where vesicular LAT co-localized with SLP-76. Indeed, the level of phosphorylated LAT within a microcluster of SLP-76 inversely correlated with the time since the last interaction between that cluster of SLP-76 and vesicles containing LAT. Finally, negative signals by Ig-like transcript 2 (ILT2) disrupted assembly of SLP-76 microclusters. Together, these data determine that movement of vesicles containing LAT is linked to the organisation of protein microclusters and suggests an important role for vesicular LAT in the SLP-76 signalosome.

Introduction

T cells become activated via the interaction of T cell receptors (TCRs) with antigen-derived peptides bound to integral membrane proteins encoded by major histocompatibility complex (MHC) class I or class II genes (pMHCs). Ligation induces phosphorylation of the TCR complex via CD4- and CD8-p56lck complexes leading to the recruitment of ZAP-70 and phosphorylation of multiple downstream adaptor proteins including LAT and SLP-76, the latter associating with GADS (*1-6*). Early imaging studies demonstrated that T cell activation is often accompanied by micrometer-scale clustering of proteins at the interface with antigen presenting cells (APC) (*7, 8*), as also visualized at other immune cell contacts (*9, 10*). More recent higher resolution imaging has revealed smaller aggregates of protein termed microclusters within the T cell immune synapse (IS) (*11-17*). Importantly, TCR signaling is initiated in such microclusters (*15-18*), and the signals are terminated as microclusters move from the periphery to the centre of the IS (*14, 15*). Signaling by inhibitory NK cell receptors is also largely confined to small domains within the IS (*18*) which can be important for how activating and inhibitory signals are integrated (*19*). The full range of heterogeneity, localization and dynamics of microcluster formation is at an early stage of discovery.

Building on the approach previously established by Bunnell, Samelson, their collaborators and others (*15-17*), we set out to address this issue by using multi-color live-cell microscopy to visualize the supramolecular organization of fluorescent protein-tagged ZAP-70, SLP-76, GADS

and LAT during T cell activation. We found that ZAP-70, LAT, or SLP-76 form separate clusters in response to TCR ligation with ZAP-70 and SLP-76 found primarily at the cell surface and a substantial fraction of LAT in sub-synaptic vesicles. Vesicles rich in LAT trafficked rapidly between surface clusters of SLP-76 where they underwent decreased motility and where phosphorylated LAT (pY191 and pY226) was enriched. In this system using anti-CD3 coated coverslips, ZAP-70 formed an array of immobile clusters at the activating surface within which vesicles containing LAT moved. We also determined that negative signaling via Ig-like transcript 2 (ILT2) disrupted the formation of both ZAP-70 and SLP-76 microclusters. Thus, these data suggest that signaling at the IS can involve interactions between sub-synaptic vesicles and cell surface microclusters.

Results

Discrete clusters of adaptors assemble at the T cell IS

Microclusters of proteins containing the central adaptor protein SLP-76 are continuously generated at the periphery of the IS following the initial phase of T cell spreading in response to antigen (*14-17*). Here, we followed the organization of proteins associated with the SLP-76 'signalosome' by co-expressing YFP-tagged SLP-76 pair-wise with adaptor proteins LAT or GADS tagged with red fluorescent mCherry. Anti-CD3 mAb immobilized on glass coverslips was used to stimulate Jurkat T cell transfectants, as used previously by others (*11, 13*). Images were acquired after the initial antigen-induced spreading response, specifically to consider how T cell signaling is sustained. Activation-induced clusters of mCherry-tagged GADS co-localized and co-migrated with SLP-76-YFP microclusters (Fig. 1*A* and Movie S1). This is consistent with constitutive SH3 domain-mediated association of GADS and SLP-76 (*6*). In striking contrast, LAT and its binding partner SLP-76 segregated into separate puncta with distinct dynamics (Fig. 1*B* and Movie S2). Intriguingly, LAT clusters moved between distinct clusters of SLP-76 and co-localized or juxtapositioned for prolonged periods of time (Fig. 1*C* and Movie S3).

We next examined the organization of these same sets of proteins within intercellular synapses between Jurkat T cells and superantigen-pulsed Raji B cells. For this, we utilized our recently described approach of orienting T cell/APC conjugates vertically with optical tweezers to obtain high-resolution images of intercellular immune synapses (*20*). In agreement with the images using antibody-coated slides, images of T cell/APC interfaces revealed that GADS co-localized

with SLP-76 whereas LAT organized within domains that were largely segregated from SLP-76 (Fig. 1*D, E*). Quantitatively, the Pearson's correlation coefficient, Rr, was 0.76 ± 0.03 for GADS and SLP-76 and only 0.19 ± 0.07 for LAT and SLP-76 (n>10).

LAT accumulates within sub-synaptic vesicles

The TCR is known to cycle between plasma membrane and vesicular compartments in resting and activated T cells (*21*). Similarly, TCR-associated signalling molecules, including LAT and SLP-76 have been shown to be present both at the plasma membrane and within intracellular vesicles. A fraction of SLP-76 can accumulate in vesicles upon T cell activation, whereas vesicles containing LAT exist in resting T cells (*3, 12, 21-23*). To investigate whether some of the observed protein 'clusters' represented membrane-proximal cytoplasmic vesicles, rather than proteins directly bound to the cell surface, we stained SLP-76-transfected Jurkat T cells with the fluorescent lipid DiI and let cells rest for 12 hours in order to allow for internalization and dispersion of DiI into cytoplasmic vesicles (Supplementary Fig. S1). From this, it was clear that SLP-76 predominantly localized in clusters distinct from DiI-stained vesicles (Fig. 2*A*) in Jurkat T cells stimulated with activating surfaces. Instead, plasma membrane-proximal vesicles stained by DiI were seen to move between the clusters of SLP-76 and would transiently co-localize. Analogous behaviour was seen for plasma membrane-proximal vesicles stained by DiI at intercellular immune synapses in live Jurkat T cell/Raji conjugates (Fig. 2*B*). A substantial fraction of LAT (but not SLP-76) clearly localized to DiI-stained vesicles within a confocal 'optical slice', i.e. within ~500 nm, of the interface between Jurkat T cells and activating surfaces (Fig. 2*C* and Movie S4). Quantitatively, we found that 30 ± 7% of LAT exists within intracellular compartments in resting T cells, consistent with previous reports (*22*). We observed

that this percentage increased upon stimulation by antigenic surfaces (supplementary Fig. S2), consistent with increased c-Cbl mediated internalization of activated LAT (*24*). In contrast, little phosphorylated LAT was detected within intracellular compartments in activated cells, confirming that active LAT is primarily present at the T cell plasma membrane (Fig S2).

Studies of T cell synapses by total internal reflection fluorescence microscopy (TIRF) microscopy have demonstrated that LAT accumulates in microclusters at the T cell plasma membrane (*15, 16*). These surface microclusters are not easily revealed by confocal microscopy, due to the worse signal-to-noise ratio compared to the thinner optical section obtained by TIRF microscopy. We therefore used TIRF microscopy to clarify whether LAT imaged by confocal microscopy was distinct from cell-surface microclusters**.** Jurkat T cell transfectants expressing fluorescent-tagged LAT or SLP-76 were imaged initially by TIRF microscopy to identify membrane associated proteins (penetration depth ~130 nm), followed by wide-field microscopy which would additionally reveal surface-proximal vesicles (depth of focus ~500 nm) in the same cells (Fig. 2*D, E*). For LAT, TIRF microscopy identified surface microclusters, as previously described (*15, 16*). Wide-field microscopy could not detect many of the LAT microclusters, due to increased background fluorescence within the thicker optical section, but instead identified a significant accumulation of LAT deeper within the cell, i.e. in membrane-proximal cytoplasmic vesicles, not detected by TIRF microscopy (Fig. 2*D*). In contrast, most clusters of SLP-76 imaged by wide-field microscopy (~90%) co-localized with clusters also imaged by TIRF microscopy, indicating that most SLP-76 was within surface microclusters (Fig. 2*E*)**.**

To further determine the nature of LAT-containing vesicles, we compared the location of LAT with markers for different vesicular compartments. We found that 70% of vesicles containing LAT-mCherry also contained GFP-Rab7, suggesting that LAT was localized in late endosomes (Fig. 2*F*). 22% of vesicles containing LAT-mCherry contained GFP-Rab8a, indicating some of the vesicles containing LAT are those trafficking directly from the Golgi to plasma membrane (Fig. 2*F*). This suggests that most vesicular LAT has been internalized from the cell surface into Rab7-positive vesicles, while a smaller fraction is nascent LAT in Rab8a-positive vesicles.

Imaging by others suggested that clusters of SLP-76 are first internalized into cytoplasmic vesicles, such that they are not detected by TIRF microscopy, before being mobile (*12*). Consistent with this, we also found that some (<10%) SLP-76 microclusters disappeared from the plasma membrane, imaged by TIRF microscopy, while migrating from the periphery to the centre of the IS. However, microclusters of SLP-76 could also remain plasma membrane-associated, i.e. be detected by TIRF microscopy, and be motile, generally moving centripetally (Fig 2*H* and Movie S5). Clusters of SLP-76 aligned with a radial arrangement of microtubules at the activating interface (Supplementary Figure S3), consistent with the centripetal movement of SLP-76 being directed by the cytoskeleton, although this remains to be confirmed experimentally.

Association of vesicular LAT with surface microclusters of SLP-76

Next, we tracked the speeds and trajectories of individual protein clusters with a view to assessing their interactions. Microclusters of SLP-76 formed at the periphery of the T cell/coverslip interface and migrated towards the centre (Fig. 3*A*), as described previously (*11,*

13, 15, 17). Trajectories of microclusters of GADS fully coincided with those of SLP-76 (Fig. 3*A*). In striking contrast, vesicular LAT and vesicles marked by DiI moved rapidly between clusters of SLP-76 (Fig. 3*A*). Both vesicular LAT and vesicles stained by DiI moved significantly faster than clusters of SLP-76 (Fig. 3*B, C*; Supplementary Figure S4).

Importantly, the speed of vesicular LAT or vesicles stained by DiI was reduced by more than 50% when co-localized with microclusters of surface SLP-76 (Fig. 3*D, E*). At intercellular synapses, the speeds of vesicles and microclusters were generally faster than at contacts with antibody-coated slides but importantly, vesicles containing LAT similarly slowed when co-localized with SLP-76 microclusters (Fig. 2*F*). This implies that vesicles containing LAT slow down when co-localized with surface clusters of SLP-76. This decreased motility could be caused by direct binding between vesicular LAT and microclusters containing SLP-76, or by interactions involving other proteins within LAT-rich vesicles, or alternatively by confinement of vesicular LAT to domains where the SLP-76 microclusters locate.

Thus, we next investigated whether LAT binding to SLP-76 would directly influence the association of LAT-rich vesicles with surface clusters of SLP-76. For this, we generated a construct encoding a mutated LAT unable to interact with the SLP-76/GADS complex. Specifically, two LAT tyrosines 171 and 191 (*25*) were substituted with phenylalanine, which also disrupts the LAT-Grb2 interaction. Transfectants of the LAT-deficient variant of Jurkat, JCam2, were made to express wild-type or mutant LAT, c-terminally tagged with mCherry, together with SLP-76. Cells expressing mutant LAT showed reduced numbers of SLP-76 clusters which did not move centripetally. In contrast, transfection of wild-type LAT restored the

normal phenotype and dynamics of SLP-76 function. Importantly, for those SLP-76 clusters that did form, the duration of contact with vesicles containing mutant LAT was significantly less ($p=0.002$) than the time of contact with vesicles containing wild-type LAT (Fig. 3*G*). This determines that the reduction in speed of LAT vesicles seen upon co-localization with SLP-76 is directly influenced by the interaction between LAT and SLP-76. Thus, either the vesicles of LAT directly bind surface microclusters of SLP-76, or their movement must be confined by a mechanism that is dependent on the LAT/SLP-76/GADS interaction.

Movement of sub-synaptic vesicles is defined by the distribution of ZAP-70

LAT is phosphorylated by the protein tyrosine kinase ZAP-70 (*3*) and therefore, we next investigated how ZAP-70 was organized in relation to vesicular LAT. In T cells activated by surfaces coated with anti-CD3 mAb OKT-3, ZAP-70 formed an array of clusters that did not show any directed movement, as previously described (*26*). Surprisingly, the movement of sub-synaptic vesicles stained by DiI and of vesicular LAT appeared restricted by the presence of ZAP-70 clusters (Fig. 4*A, B* and Movie S6, Movie S7). Specifically, vesicles moved along paths in-between clusters of ZAP-70. Previously it has been demonstrated that activation of T cells by immobilized anti-CD3 mAb lead to formation of immobile surface clusters of the TCR (*27*). Here, clusters of ZAP-70 co-localized with such stationary clusters of TCR (Fig 4*C*). This is consistent with immobile clusters of ZAP-70 representing sites of TCR signaling. The movement of vesicles containing LAT between such clusters demonstrates that these vesicles are tightly coupled to the architecture of the immune synapse and in particular to the organization of TCR/ZAP-70 signaling complexes.

Phosphorylation of LAT at SLP-76 clusters

To assess the activation state of LAT, we stained transfectants with Ab against phosphorylated forms of LAT, specifically pY191 or pY226 (*22*). In transfectants expressing fluorescent protein-tagged SLP-76 and LAT, LAT phosphorylated at Y191 or Y226 was detected in clusters where LAT and SLP-76 co-localized (Fig. 5*A-D*). Clusters of SLP-76 away from large puncta of LAT were associated with lower levels of phosphorylated LAT, whereas LAT away from SLP-76 very rarely contained any detectable phosphorylated LAT (Fig. 5*C, D*). Results were similar when cells were additionally stained with DiI, which identified LAT 'puncta' as sub-synaptic vesicles (Supplementary Fig. 5A).

We next related the extent of LAT phosphorylation in SLP-76 clusters to the history of interactions between SLP-76 clusters and vesicles containing LAT. The dynamics of SLP-76 and LAT were imaged in individual live cells followed by fixation of these cells and staining for phospho-LAT. The intensity of LAT phosphorylation within individual clusters of SLP-76 was then related to the time elapsed since the last interaction with puncta of LAT. This analysis revealed that higher levels of LAT phosphorylation occurred within those clusters of SLP-76 which had more recent interactions with puncta of LAT. Indeed, the extent of phospho-LAT staining inversely correlated with the time since the last interaction between puncta of SLP-76 and LAT. Results were similar when cells were additionally stained with DiI, to identify the 'puncta' of LAT as vesicles (Supplementary Fig. 5B). These data suggest that phosphorylation of LAT within clusters of SLP-76 is intimately linked to the transient co-localization of vesicles containing LAT with surface SLP-76.

Negative signaling through ILT2 inhibits microcluster formation

We next set out to test how negative signals impact the formation of microclusters and the sub-synaptic vesicular compartment of LAT localization. The inhibitory receptor ILT2 (also known as LIR-1, LIRB1, and CD85j) is expressed on subsets of NK cells and T cells and binds a broad spectrum of class I MHC proteins (*28*). In T cells, ligation of ILT2 reduces antigen-induced TCR signal transduction and actin polymerization (*29*). Ligation of ILT2, expressed in Jurkat transfectants, inhibited the formation of ZAP-70 microclusters upon stimulation by surfaces coated with anti-CD3 mAb OKT-3 (Fig. 6*A*). Ligation of ILT2 also lead to a large reduction in the number of SLP-76 clusters formed (Fig. 6*B*), likely a direct consequence of ZAP-70 cluster formation being abrogated. In the few cells which did form SLP-76 clusters, movement of these clusters was restricted to small distances back and forth and not directed to the centre of the interface (Fig. 6*C*). Furthermore, ILT2 engagement reduced the speed of vesicles containing LAT (Fig. 6*D*). No significant difference was then detected between the speed of free LAT and LAT associated-with SLP-76 clusters when ILT2 was ligated. In live conjugates of superantigen-pulsed APCs with ILT2-transfected Jurkat T cells, ILT2 clustered at the APC/T cell interface and inhibited the formation of SLP-76 microclusters at the IS (Fig. 6*E*). Inhibition of SLP-76 cluster formation could be overcome by blocking ILT2 ligation by using a mAb against class I MHC protein (Fig. 6*F*). Therefore as a prototype for the action of negative receptors, ILT2 interrupted the assembly of microclusters at the IS. Similarly, negative signaling upon CTLA-4 ligation has recently been also been shown to inhibit ZAP-70 clustering (*30*), indicating that the action of inhibitory receptors on T cells may generally act upstream of the formation of protein microclusters.

Discussion

Here we describe the dynamics of distinct assemblies of functionally connected TCR-proximal signaling components SLP-76, LAT, and ZAP-70 at the IS. The adaptor protein LAT is an integral plasma membrane protein that links antigen recognition by the TCR with several key downstream signalling components (*1, 31*). High-resolution imaging studies have shown that antigen receptors and LAT are organized in distinct domains at the plasma membrane, which juxtaposition, but remain separate, upon antigenic stimulation (*32, 33*). LAT functionality therefore involves the spatio-temporal regulation of protein assemblies. Moreover, a significant fraction of LAT has been shown previously to accumulate within intracellular vesicles (*3, 21, 22*). Here we found that dynamics of LAT in sub-synaptic vesicles was strikingly governed by the architecture of the IS. Specifically, the movement of LAT-containing vesicles was confined to tracks between ZAP-70-containing microclusters representing the TCR activation sites. Perhaps more importantly, LAT found in sub-synaptic vesicles frequently associated with clusters of plasma membrane-associated SLP-76, where the movement of vesicles was temporarily confined. These interactions correlated with sites of LAT phosphorylation, visualized by immuno-fluorescent staining with phospho-specific mAb. Indeed, the extent of phospho-LAT staining within a microcluster of SLP-76 inversely correlated with the time since the last interaction between that cluster of SLP-76 and vesicles containing LAT. Taken together, these data imply an important role for vesicular LAT in the SLP-76 signalosome. Specifically, these data suggest that phosphorylation of LAT is triggered where vesicular pools of LAT meet surface microclusters of SLP-76 at the plasma membrane.

There are several possible mechanisms by which vesicular LAT could slow down when colocalized with SLP-76. First, the movement of sub-synaptic vesicles is reminiscent of the tracks by individual molecules of CD45, Lck, and surface LAT within the plasma membrane, which revealed membrane microdomains resulting from protein-protein networks that can exclude or trap signaling molecules (*27*). Thus, specific protein-protein binding can create the observed confinement of vesicular LAT and this could be direct binding between LAT and SLP-76/GADS. In support of this, vesicles containing mutant LAT lacking tyrosines 171 and 191 (critical for the binding of GADS and Grb2) demonstrated significantly reduced time of association with surface clusters of SLP-76, potentially resulting from the inhibition of direct binding of vesicular LAT to surface SLP-76/GADS. Alternatively, since TCR activation sites are directly linked to the cytoskeleton (*11*), the activating T cell surface may be partitioned into distinct microdomains via the involvement of actin-based membrane-skeleton "fences" (*34*). It is possible that such cytoskeletal corals could confine the movement of vesicles, potentially promoting interactions with surface clusters of protein trapped within the same microdomain. However, this remains to be tested, as part as the broader aim to establish how vesicles containing LAT are trafficked.

While the correlation between LAT translocation to surface SLP-76, its phosphorylation, decrease in motility and the stable association of phospho-LAT with SLP-76 is consistent with the biochemical cascade outlined in previous studies, our data demonstrate that interaction between the IS and the sub-synaptic vesicular compartment could facilitate a novel physical basis for spatio-temporal control of the active SLP-76 signalosome. Though the functional implication of the interaction between LAT-containing vesicles and surface clusters of SLP-76

remains to be investigated, it is possible that surface clusters of SLP-76 can 'perceive' vesicular LAT differentially from LAT in the plasma membrane, due the inverted presentation of the LAT cytoplasmic domain when presented in *trans* (or anti-parallel) compared to the conventional *cis* (parallel) interaction that would occur for proteins tethered to the same membrane. Regulating the interaction between vesicles and surface protein clusters could therefore play an important role in limiting or promoting interactions between signaling proteins. Indeed, this is emerging to be the case in numerous cell biological systems (*35*).

Recent studies have indicated that T cell costimulatory signals mediated by the adhesion molecule VLA-4 act to alter the migratory dynamics at the IS of key signaling molecules such that interactions between macromolecular clusters of SLP-76 and its regulating kinase ZAP-70 are dramatically prolonged (*26*). Here we demonstrate that the negative signal generated by the inhibitory receptor ILT2 is able to inhibit the macromolecular assembly of ZAP-70 and SLP-76 clusters as well as the dynamics and interactions of remaining SLP-76 microclusters with sub-synaptic LAT. These observations are consistent with the known biochemical effects of ILT2 in reducing TCR phosphorylation and disrupting cytoskeletal rearrangements. Thus, regulating the assembly and dynamics of such supramolecular interactions may be a common mechanism utilized by accessory receptors in modifying the primary immune signaling cascade. Overall, an emerging new theme is that interactions between immune cell kinases and adaptors can be controlled by the dynamics of supramolecular assemblies rather than isolated protein-protein interactions.

Materials and methods

Cell culture and constructs

Jurkat T cells (ATCC, Manassas, VA) were grown in R10 medium (RPMI-1640 with 10% FCS, 2 mM L-glutamine, and penicillin/streptomycin). LAT-deficient JCam2 were a kind gift from A. Weiss. Plasmids encoding Rab5, Rab8a, and Rab7 fluorescent constructs were kind gifts from M.C. Seabra. GADS, ILT2, LAT, SLP-76, and ZAP-70 were amplified from human cDNA. SLP-76 was cloned into pEYFP-N1 (Clontech, Mountain View, CA). GADS, ILT2, LAT, and ZAP-70 were c-terminally tagged by cloning into pcDNA3.1 (Invitrogen, Paisley, UK) containing mCherry, Citrine, or mCFP. Cells were transfected by microporation (Digital Bio Technology, Seoul, South Korea), using a single pulse of 30 ms, 1380 V. All experiments investigating SLP-76-YFP were performed in both wild-type Jurkat T cells and SLP-76 deficient mutant Jurkat cell line J14. Unless indicated otherwise only the data-set for wild-type Jurkat T cells is shown, with data for J14 cells being equivalent.

Imaging

Polylysine (Sigma, Poole, UK) treated chambered coverslides (Nunc, Rochester, NY) were coated with 10 μg ml^{-1} anti-CD3 mAb OKT-3 (ATCC) or with both 10 μg ml^{-1} OKT-3 and 10 μg ml^{-1} anti-ILT2 mAb (R&D Systems, Minneapolis, MN) for 1 hr at 37°C to generate T cell-activating surfaces, and blocked with R10 medium for 10 min. Cells were imaged by resonance scanning confocal microscopy using laser lines of 405, 488, 514, 546, and 594 nm and a 63x 1.2NA water immersion objective (TCS SP5 RS, Leica, Heidelberg, Germany). Images were acquired using Leica Application Suite Advanced Fluorescence (Leica, Heidelberg, Germany)

software. Simultaneous imaging of different fluorophores was by sequential line scanning. Immune synapses within T cell/APC conjugates were imaged at high resolution by orientating cells using optical tweezers, as recently described (*20*). Such optical tweezers were generated by coupling an infra-red laser beam (980 nm) into the non-scanned beam path of a commercially available confocal microscope (Leica TCS SP5), with minimum effect on the cells due to low water absorption at this wavelength. Tweezers could be moved in all three dimensions using simple optics such as activatable mirrors (xy) and translatable lenses (z). Importantly, confocal imaging could be performed with no restriction during manipulation of cell conjugates, therefore allowing imaging of intercellular T cell/APC immune synapses at full speed (> 1fps) and resolution (250nm). Total internal reflection fluorescence microscopy was performed using laser lines 473 nm or 532 nm directed through an epi-fluorescence microscope (IX71, Olympus, Tokyo, Japan) fitted with a 60x 1.45NA oil immersion objective. The penetration depth of the evanescent wave at the normalised intensity 1/*e* was calculated to be ~130 nm. To mark vesicles, cells were stained with 1 μM membrane dye 1,1-dioctadecyl-3,3,3,3-tetramethylindocarbocyanine perchlorate (Vybrant DiI; Invitrogen) in R10 medium for 30 min at 37°C, washed and then left to internalise DiI overnight at 37°C. For Jurkat/Raji conjugate formation Raji B cells (ATCC) were pulsed with 100 ng ml^{-1} Staphylococcus enterotoxin E (SEE) superantigen (Toxin Technology) for 1hr. To fix, cells that were activated for 10 min (Jurkat/Raji conjugates or OKT-3-coated surface-activated Jurkat T cells) were incubated in 2% paraformaldehyde/0.1% Gluteraldehyde (Sigma) for 2 min at room temperature. To stain, fixed cells were permeabilized with 0.5% Triton/PBS (Sigma) for 1 min and blocked for 1 hr with 5% horse serum. Cells were stained for 1 hr at 4°C with 1 μg/ml rabbit polyclonal primary antibody, including anti-phospho-ZAP-70 Y319, (Cell Signaling Technology, Danvers, MA), anti-phospho-LAT Y191 (Upstate), anti-phospho-LAT Y226 (Millipore, Watford, UK), rabbit IgG isotype control (Invitrogen), followed by 1 hr at 4°C with

Alexa Fluor-405 labelled goat anti-rabbit IgG secondary Ab (Invitrogen). Images were analysed with Leica confocal software (LCS; Leica), Volocity (Improvision, Coventry, UK), or ImageJ (National Institutes of Health, Bethesda, MA) software. Pearson's correlation coefficient (Rr) was calculated by intensity correlation analysis of the images in ImageJ. Live-cell images were acquired at 37°C, 5% CO_2, using R10 as imaging medium.

Supplementary Material Titles

Figure S1 **DiI-stained intracellular vesicles positioned proximal to the immune synapse**

Figure S2 **Intracellular fraction of LAT**

Figure S3 **Clusters of SLP-76 align with the microtubule cytoskeleton**

Figure S4 **Protein cluster speeds at the interface between Jurkat T cells and OKT-3-coated coverslips**

Figure S5 **LAT phosphorylation at the site of SLP-76 contact with vesicular LAT**

Movie S1 **Dynamics of SLP-76 and GADS**

Movie S2 **Dynamics of SLP-76 and LAT**

Movie S3 **Dynamics of a single LAT cluster**

Movie S4 **Dynamics of SLP-76, LAT, and intracellular vesicles**

Movie S5 **Dynamics of SLP-76 clusters imaged by TIRF**

Movie S6 **Dynamics of sub-synaptic vesicles in relation to clusters of ZAP-70**

Movie S7 **Dynamics of vesicular LAT in relation to clusters of ZAP-70**

References

1. C. E. Rudd, Adaptors and molecular scaffolds in immune cell signaling. *Cell* **96,** 5-8 (1999).

2. M. Raab, A. J. da Silva, P. R. Findell and C. E. Rudd, Regulation of Vav-SLP-76 binding by ZAP-70 and its relevance to TCR zeta/CD3 induction of interleukin-2. *Immunity* **6,** 155-164 (1997).

3. W. Zhang, J. Sloan-Lancaster, J. Kitchen, R. P. Trible and L. E. Samelson, LAT: the ZAP-70 tyrosine kinase substrate that links T cell receptor to cellular activation. *Cell* **92,** 83-92 (1998).

4. J. B. Wardenburg, C. Fu, J. K. Jackman, H. Flotow, S. E. Wilkinson, D. H. Williams, R. Johnson, G. Kong, A. C. Chan and P. R. Findell, Phosphorylation of SLP-76 by the ZAP-70 protein-tyrosine kinase is required for T-cell receptor function. *J Biol Chem* **271,** 19641-19644 (1996).

5. H. Asada, N. Ishii, Y. Sasaki, K. Endo, H. Kasai, N. Tanaka, T. Takeshita, S. Tsuchiya, T. Konno and K. Sugamura, Grf40, A novel Grb2 family member, is involved in T cell signaling through interaction with SLP-76 and LAT. *J Exp Med* **189,** 1383-1390 (1999).

6. S. K. Liu, N. Fang, G. A. Koretzky and C. J. McGlade, The hematopoietic-specific adaptor protein gads functions in T-cell signaling via interactions with the SLP-76 and LAT adaptors. *Curr Biol* **9,** 67-75 (1999).

7. A. Grakoui, S. K. Bromley, C. Sumen, M. M. Davis, A. S. Shaw, P. M. Allen and M. L. Dustin, The immunological synapse: a molecular machine controlling T cell activation. *Science* **285,** 221-227 (1999).

8. C. R. Monks, B. A. Freiberg, H. Kupfer, N. Sciaky and A. Kupfer, Three-dimensional segregation of supramolecular activation clusters in T cells. *Nature* **395,** 82-86 (1998).

9. D. M. Davis, I. Chiu, M. Fassett, G. B. Cohen, O. Mandelboim and J. L. Strominger, The human natural killer cell immune synapse. *Proc Natl Acad Sci U S A* **96,** 15062-15067 (1999).

10. F. D. Batista, D. Iber and M. S. Neuberger, B cells acquire antigen from target cells after synapse formation. *Nature* **411,** 489-494 (2001).

11. M. Barda-Saad, A. Braiman, R. Titerence, S. C. Bunnell, V. A. Barr and L. E. Samelson, Dynamic molecular interactions linking the T cell antigen receptor to the actin cytoskeleton. *Nat Immunol* **6,** 80-89 (2005).

12. V. A. Barr, L. Balagopalan, M. Barda-Saad, R. Polishchuk, H. Boukari, S. C. Bunnell, K. M. Bernot, Y. Toda, R. Nossal and L. E. Samelson, T-cell antigen receptor-induced signaling complexes: internalization via a cholesterol-dependent endocytic pathway. *Traffic* **7,** 1143-1162 (2006).

13. S. C. Bunnell, A. L. Singer, D. I. Hong, B. H. Jacque, M. S. Jordan, M. C. Seminario, V. A. Barr, G. A. Koretzky and L. E. Samelson, Persistence of cooperatively stabilized signaling clusters drives T-cell activation. *Mol Cell Biol* **26,** 7155-7166 (2006).

14. R. Varma, G. Campi, T. Yokosuka, T. Saito and M. L. Dustin, T cell receptor-proximal signals are sustained in peripheral microclusters and terminated in the central supramolecular activation cluster. *Immunity* **25,** 117-127 (2006).

15. T. Yokosuka, K. Sakata-Sogawa, W. Kobayashi, M. Hiroshima, A. Hashimoto-Tane, M. Tokunaga, M. L. Dustin and T. Saito, Newly generated T cell receptor microclusters initiate and sustain T cell activation by recruitment of Zap70 and SLP-76. *Nat Immunol* **6,** 1253-1262 (2005).

16. G. Campi, R. Varma and M. L. Dustin, Actin and agonist MHC-peptide complex-dependent T cell receptor microclusters as scaffolds for signaling. *J Exp Med* **202,** 1031-1036 (2005).

17. S. C. Bunnell, D. I. Hong, J. R. Kardon, T. Yamazaki, C. J. McGlade, V. A. Barr and L. E. Samelson, T cell receptor ligation induces the formation of dynamically regulated signaling assemblies. *J Cell Biol* **158,** 1263-1275 (2002).

18. B. Treanor, P. M. Lanigan, S. Kumar, C. Dunsby, I. Munro, E. Auksorius, F. J. Culley, M. A. Purbhoo, D. Phillips, M. A. Neil, D. N. Burshtyn, P. M. French and D. M. Davis, Microclusters of inhibitory killer immunoglobulin-like receptor signaling at natural killer cell immunological synapses. *J Cell Biol* **174,** 153-161 (2006).

19. F. J. Culley, M. Johnson, J. H. Evans, S. Kumar, R. Crilly, J. Casasbuenas, T. Schnyder, M. Mehrabi, M. P. Deonarain, D. S. Ushakov, V. Braud, G. Roth, R. Brock, K. Kohler and D. M. Davis, Natural killer cell signal integration balances synapse symmetry and migration. *PLoS Biol* **7,** e1000159 (2009).

20. S. Oddos, C. Dunsby, M. A. Purbhoo, A. Chauveau, D. M. Owen, M. A. Neil, D. M. Davis and P. M. French, High-speed high-resolution imaging of intercellular immune synapses using optical tweezers. *Biophys J* **95,** L66-68 (2008).

21. H. Liu, M. Rhodes, D. L. Wiest and D. A. Vignali, On the dynamics of TCR:CD3 complex cell surface expression and downmodulation. *Immunity* **13,** 665-675 (2000).

22. G. Bonello, N. Blanchard, M. C. Montoya, E. Aguado, C. Langlet, H. T. He, S. Nunez-Cruz, M. Malissen, F. Sanchez-Madrid, D. Olive, C. Hivroz and Y. Collette, Dynamic recruitment of the adaptor protein LAT: LAT exists in two distinct intracellular pools and controls its own recruitment. *J Cell Sci* **117,** 1009-1016 (2004).

23. M. C. Montoya, D. Sancho, G. Bonello, Y. Collette, C. Langlet, H. T. He, P. Aparicio, A. Alcover, D. Olive and F. Sanchez-Madrid, Role of ICAM-3 in the initial interaction of T lymphocytes and APCs. *Nat Immunol* **3,** 159-168 (2002).

24. L. Balagopalan, V. A. Barr, C. L. Sommers, M. Barda-Saad, A. Goyal, M. S. Isakowitz and L. E. Samelson, c-Cbl mediated regulation of LAT-nucleated signaling complexes. *Mol Cell Biol* (2007).

25. W. Zhang, R. P. Trible, M. Zhu, S. K. Liu, C. J. McGlade and L. E. Samelson, Association of Grb2, Gads, and phospholipase C-gamma 1 with phosphorylated LAT tyrosine residues. Effect of LAT tyrosine mutations on T cell angigen receptor-mediated signaling. *J Biol Chem* **275,** 23355-23361 (2000).

26. K. Nguyen, N. R. Sylvain and S. C. Bunnell, T cell costimulation via the integrin VLA-4 inhibits the actin-dependent centralization of signaling microclusters containing the adaptor SLP-76. *Immunity* **28,** 810-821 (2008).

27. A. D. Douglass and R. D. Vale, Single-molecule microscopy reveals plasma membrane microdomains created by protein-protein networks that exclude or trap signaling molecules in T cells. *Cell* **121,** 937-950 (2005).

28. M. Colonna, F. Navarro, T. Bellon, M. Llano, P. Garcia, J. Samaridis, L. Angman, M. Cella and M. Lopez-Botet, A common inhibitory receptor for major histocompatibility complex class I molecules on human lymphoid and myelomonocytic cells. *J Exp Med* **186,** 1809-1818 (1997).

29. J. Dietrich, M. Cella and M. Colonna, Ig-like transcript 2 (ILT2)/leukocyte Ig-like receptor 1 (LIR1) inhibits TCR signaling and actin cytoskeleton reorganization. *J Immunol* **166,** 2514-2521 (2001).

30. H. Schneider, X. Smith, H. Liu, G. Bismuth and C. E. Rudd, CTLA-4 disrupts ZAP70 microcluster formation with reduced T cell/APC dwell times and calcium mobilization. *Eur J Immunol* **38,** 40-47 (2008).

31. C. S. Guy and D. A. Vignali, Organization of proximal signal initiation at the TCR:CD3 complex. *Immunol Rev* **232,** 7-21 (2009).

32. B. S. Wilson, J. R. Pfeiffer, Z. Surviladze, E. A. Gaudet and J. M. Oliver, High resolution mapping of mast cell membranes reveals primary and secondary domains of Fc(epsilon)RI and LAT. *J Cell Biol* **154,** 645-658 (2001).

33. B. F. Lillemeier, M. A. Mortelmaier, M. B. Forstner, J. B. Huppa, J. T. Groves and M. M. Davis, TCR and Lat are expressed on separate protein islands on T cell membranes and concatenate during activation. *Nat Immunol* **11,** 90-96 (2010).

34. A. Kusumi, C. Nakada, K. Ritchie, K. Murase, K. Suzuki, H. Murakoshi, R. S. Kasai, J. Kondo and T. Fujiwara, Paradigm shift of the plasma membrane concept from the two-dimensional continuum fluid to the partitioned fluid: high-speed single-molecule tracking of membrane molecules. *Annu Rev Biophys Biomol Struct* **34,** 351-378 (2005).

35. G. Scita and P. P. Di Fiore, The endocytic matrix. *Nature* **463,** 464-473 (2010).

Acknowledgements

We thank Matthew J. Hannah (National Institute for Medical Research, London) for pointing out the possibility of differences in anti-parallel versus parallel recognition of LAT. We are grateful to M. Seabra for kind gifts of plasmids as indicated. We thank Nigel Burroughs and members of our laboratories for helpful discussions and Martin Spitaler for assistance in our core microscope facility (FILM). This work was supported by the Biotechnology and Biological Science Research Council, the Medical Research Council, the Chemical Biology Centre, a Lister Institute Research Prize (to D.M.D.), and Wolfson Royal Society Research Merit Awards (to P.M.W.F and D.M.D).

Figure legends

Figure 1: Heterogeneity in T cell protein clusters. *A-D*) Images show distribution of protein clusters at the interface between transfected Jurkat T cells and OKT-3-coated coverslips. *A*) Distribution of SLP-76-YFP (green) and GADS-mCherry (red) in Jurkat T cells. The cell was imaged 2 minutes after contact with the coverslip. *B*) Distribution of SLP-76-YFP (green) and LAT-mCherry (red) in Jurkat T cells. Interference reflection microscopy (IRM) image indicates extent of T cell/coverslip interface. The cell was imaged 2.5 minutes after contact with the coverslip. *C*) Movement of a cluster of LAT (red) between four separate SLP-76 clusters (green) over 3 min. Arrows indicate direction of LAT movement. Right panel traces the movement of these LAT and SLP clusters over the entire time-course. *D, E*) Distribution of proteins at the immune synapse formed between a transfected Jurkat T cell and a SEE-pulsed Raji B cell. Fixed conjugates were oriented to be upright using optical tweezers for high-resolution imaging of the intercellular synapse. *D*) Distribution at the immune synapse of SLP-76-YFP (Green) and LAT-mCherry (red) or *E*) SLP-76-YFP (Green) and GADS-mCherry (red). Pearson's correlation coefficients (Rr) are shown in merged images (as mean ± S.E.M.). Scale bars: 10 μm, except in panel *B*: 2 μm. Panels are representative of at least 10 cells each.

Figure 2: LAT accumulates within membrane-proximal cytoplasmic vesicles. *A*) Distribution of SLP-76-YFP (green) and cytoplasmic vesicles marked by membrane dye DiD (red) at the interface between transfected Jurkat T cells and OKT-3-coated coverslips. *B*) Distribution of SLP-76-YFP (green) and cytoplasmic vesicles (red) at the intercellular synapse between Jurkat T cell transfectant and superantigen (SEE)-pulsed Raji B cell. Jurkat T cells were stained with DiD to visualize cytoplasmic vesicles. *C*) Distribution of SLP-76-YFP (blue), LAT-mCherry (green), and cytoplasmic vesicles (red) at the interface between Jurkat T cells and OKT-3-coated coverslips. Jurkat T cells were transfected to express SLP-76-YFP, LAT-mCherry and vesicles were visualized with membrane dye DiI. *D, E*) Comparison of fixed cells imaged by TIRF microscopy (green) and widefield microscopy (red) of transfectants expressing *D*) LAT-mCherry or *E*) SLP-76-YFP. Yellow indicates where fluorescence from both imaging modalities was detected. *F, G*) Distribution of LAT (red) and *F*) Rab7 (green) or *G*) Rab8a (green) at the interface between fixed Jurkat T cells and OKT-3-coated coverslips. Cells were co-transfected to express LAT-mCherry and GFP-tagged Rab proteins. *H*) TIRF image of SLP-76-YFP clusters in live transfectants. Insets show translocation of selected clusters over 6 min. Separate clusters (red and green asterisks) are seen to fuse (red/green asterisk). Maximum projection (Right panel; Max. Project.) shows the tracks of all clusters over the time-course. Scale bars: 10 μm; Inset in (*B*): 2 μm; Insets in (*H*): 5 μm. Panels are representative of at least 10 cells each.

Figure 3: Dynamics of microclusters and vesicles. *A*) Microcluster and vesicle movement was tracked in cells expressing SLP-76-YFP, that were co-transfected to express GADS-mCherry (left panel), LAT-mCherry (middle panel), or stained for vesicles with the membrane dye DiI (right panel). SLP-76 tracks are shown in shades of green and overlaid with tracks of other transfected protein or membrane dye in shades of red. Measurements are separated by 5 sec. Dotted line indicates extent of T cell/coverslip interface. Arrowheads indicate final trajectory of tracks. *B*) Distance travelled by individual microclusters within cells transfected to express SLP-76-YFP (green tracks) and co-transfected to express GADS-mCherry, LAT-mCherry, or stained for vesicles with DiI. Trajectories of secondary transfected proteins/membrane dye are shown in red. *C*) Summary of individual microcluster/vesicle speeds as measured from time-lapse images. *D*) Tracks of vesicular LAT in activated Jurkat T cells transfectants expressing SLP-76-YFP and LAT-mCherry were analysed. Specifically, for each vesicle containing LAT the speed was determined when it was moving unconnected to clusters of SLP-76 ('Free LAT'), and compared to the speed when it overlapped with, or was juxtapositioned to, clusters of SLP-76 ('SLP-76 associated'). *E*) Plot shows the speeds of individual DiI-stained vesicles before and during contact with SLP-76 clusters. *F*) Plot shows the speeds of individual DiI-stained vesicles before and during contact with clusters of SLP-76 at the intercellular immune synapse formed between a Jurkat T cell and SEE-pulsed Raji B cell. These data were obtained using optical tweezers to orientate the cell-cell conjugates for high resolution imaging. *G, H)* Kymographs depicting the movement of *G)* a LAT cluster or *H)* a DiI-stained vesicle and clusters of SLP-76. Left panels in each pair show single LAT-mCherry clusters or a DiI-stained vesicle (red) and clusters of SLP-76-mYFP (green). Movement of the LAT cluster or the vesicle between the separate SLP-76

clusters is shown as kymograph in right panels. Arrow in (*H*) indicates the rapid translocation of a DiI-stained vesicle from one cluster of SLP-76 to another. Scale bar for left panels: 2 μm. Scale bars for right panels: vertical bar, 2 μm; horizontal bar, 1 min. *I*) The LAT-deficient Jurkat variant JCam2 was transfected to express SLP-76-YFP along with either mCherry-tagged wild-type LAT, or mutant LAT with two tyrosine substitutions, Y171F and Y191F. Plot compares the length of association with SLP-76 of vesicles containing wild-type or mutant LAT. Numbers above bars indicate number of LAT/SLP-76 interactions observed to have the indicated duration of contact. *B*-*F*) Graphs represent data from at least 6 cells each.

Figure 4: The movement of sub-synaptic vesicles is defined by regions where ZAP-70 clusters. Figure shows the relationship between clusters of ZAP-70 and movement of *A)* sub-synaptic vesicles or *B)* vesicular LAT in Jurkat cells stimulated on OKT-3-coated slides. *A*) Jurkat T cells transfected to express ZAP-70-mCFP (green) and stained with DiI (red). *B*) Jurkat T cells transfected to express ZAP-70-mCFP (green) and LAT-mCherry (red). Right panels show enlarged view of boxed regions and highlight the track of an exemplar vesicle or cluster of LAT (white line) tracked for at least 2 minutes. C) Fixed Jurkat T cells expressing ZAP-70-mCFP (red) and CD3ζ-YFP (green). Transfectants were activated on OKT-3-coated coverslips for 10 min before fixation. *A, B*) Images were taken every 2.5 s. As ZAP-70 clusters were extremely faint the ZAP-70 images shown are the sum of all ZAP-70 frames acquired in each experiment and were processed in ImageJ to remove background cytoplasmic ZAP-70 signal. Scale bars in left panels of *A, B)* 10 μm; 5 μm in right panels, *C)* 10 μm. Panels are representative of at least 10 cells each.

Figure 5: LAT phosphorylation at the site of contact with SLP-76 clusters. Data and images from the interface between transfected Jurkat T cells and OKT-3-coated coverslips. *A, B*) Jurkat T cell transfectants expressing SLP-76-YFP (green) and LAT-mCherry (red) activated by OKT-3-coated coverslips. Immunofluorescent staining (blue) with mAbs against LAT phosphorylated on tyrosine residue *A*) 191 or *B*) 226. *C, D*) Plots show the fluorescence intensity of phosphorylated LAT (pY191 or pY226) staining in Jurkat T cells (pY191 stain, n=11; pY226 stain, n=7) transfected to express SLP-76-YFP and LAT-mCherry after activation by anti-CD3 coated coverslips. The level of phospho-LAT staining is compared within clusters that contain LAT, SLP-76, or both LAT and SLP-76 (LAT/SLP). A region lacking clusters was analysed to determine background (backgr.) intensity for each cell. E) Jurkat T cell transfectants expressing SLP-76-mYFP and LAT-mCherry were activated by anti-CD3 coated coverslips. A single cell was selected and imaged every 3 seconds for 240 seconds. Cells were fixed and stained for phospho-LAT (pY191), and the same cell imaged live was re-imaged after fixation/staining. Plot shows fluorescence intensity above background of phospho-LAT staining within SLP-76 clusters. The live cell data was used to determine time elapsed for each SLP-76 cluster since last contact with a cluster of LAT (n = 10 cells). Bars indicate mean fluorescence intensity ± S.E.M. Scale bars: 10 μm. *A, B*) To highlight weak phospho-LAT staining corresponding images were processed in ImageJ to remove background signal. *C, D, E*) Fluorescence intensity was determined from unprocessed images.

Figure 6: Negative signaling by ILT2 inhibits microcluster formation and interactions with LAT vesicles. *A*) Formation of clusters of ZAP-70 in Jurkat T cells transfected to express ZAP-70-mCFP and ILT2-Citrine. Cells were stimulated on slides coated either with anti-CD3 mAb or a mixture of anti-CD3 and anti-ILT2 mAbs. To observe these faint clusters of ZAP-70 ten consecutive exposures were summed. *B*) Formation of clusters of SLP-76-YFP in Jurkat T cells transfected to express either SLP-76-YFP alone or SLP-76-YFP with ILT2-mCFP (indicated at top of graph). Number of SLP-76 clusters was determined at the interface between transfectants and slides coated either with anti-CD3 mAb or a mixture of anti-CD3 and anti-ILT2 mAbs (as indicated on x-axis). *C*) Jurkat T cells transfected to express LAT-mCherry, SLP-76-YFP, and ILT2-mCFP, stimulated with slides coated with a mixture of anti-CD3 and anti-ILT2 mAbs. Trace shows movement of individual SLP-76-YFP (green) and LAT-mCherry (red) clusters over 3 min. Trace of inset shows movement of clusters over a further 3 min. *D*) Plots showing the speed of LAT clusters in Jurkat T cells transfected to express LAT-mCherry, SLP-76-YFP, and ILT2-mCFP and stimulated an antibody-coated coverslips. The speed was measured separately for free LAT clusters, and those associated with clusters of SLP-76. Cells were stimulated with either anti-CD3 mAb (right graph) or a mixture of anti-CD3 and anti-ILT2 mAbs (left graph). *E*) Live cell conjugates between SEE-pulsed Raji B cells and Jurkat T cells expressing either SLP-76-YFP (top row) or SLP-76-YFP and ILT2-mCFP (bottom row). Distribution of ILT2-mCFP (red) is shown overlaid the transmission image (bottom left panel). Extent of SLP-76-YFP clustering at the synapse is highlighted by its fluorescence intensity being shown on the indicated glow-scale (right panels). *F*) Quantification of the number of SEE-pulsed Raji/Jurkat T cell conjugates which developed SLP-76 clusters at the IS. Jurkat T cells were transfected with either

SLP-76-YFP or SLP-76-YFP and ILT2-mCFP. The ILT2/MHC protein interaction was blocked in the presence of 10 μg ml^{-1} anti-class I MHC protein mAb W6/32. Cells lacking any punctate accumulation of SLP-76-YFP at the IS were scored as negative. Experiment was performed in triplicate assessing a total of 270 conjugates. Error bars on graph indicate ± S.E.M. Scale bars: 10 μm, inset 2 μm.

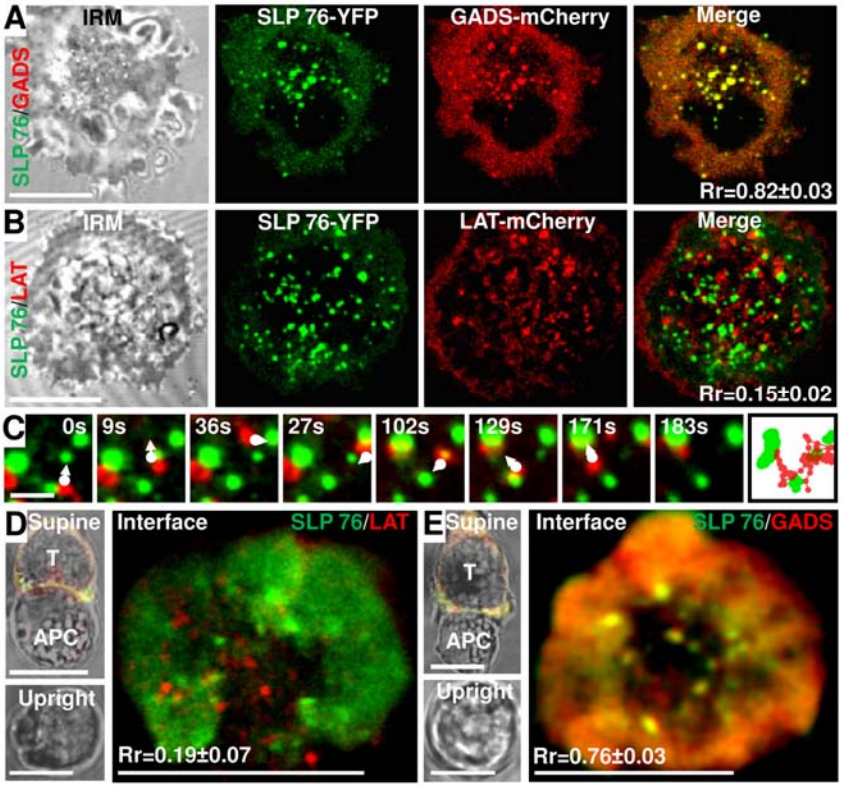
A
IRM
SLP 76-YFP
GADS-mCherry
Merge
SLP 76/GADS
Rr=0.82±0.03
B
IRM
SLP 76-YFP
LAT-mCherry
Merge
SLP 76/LAT
Rr=0.15±0.02
C
0s
9s
36s
27s
102s
129s
171s
183s
D
Supine
T
APC
Upright
Interface
SLP 76/LAT
Rr=0.19±0.07
E
Supine
T
APC
Upright
Interface
SLP 76/GADS
Rr=0.76±0.03

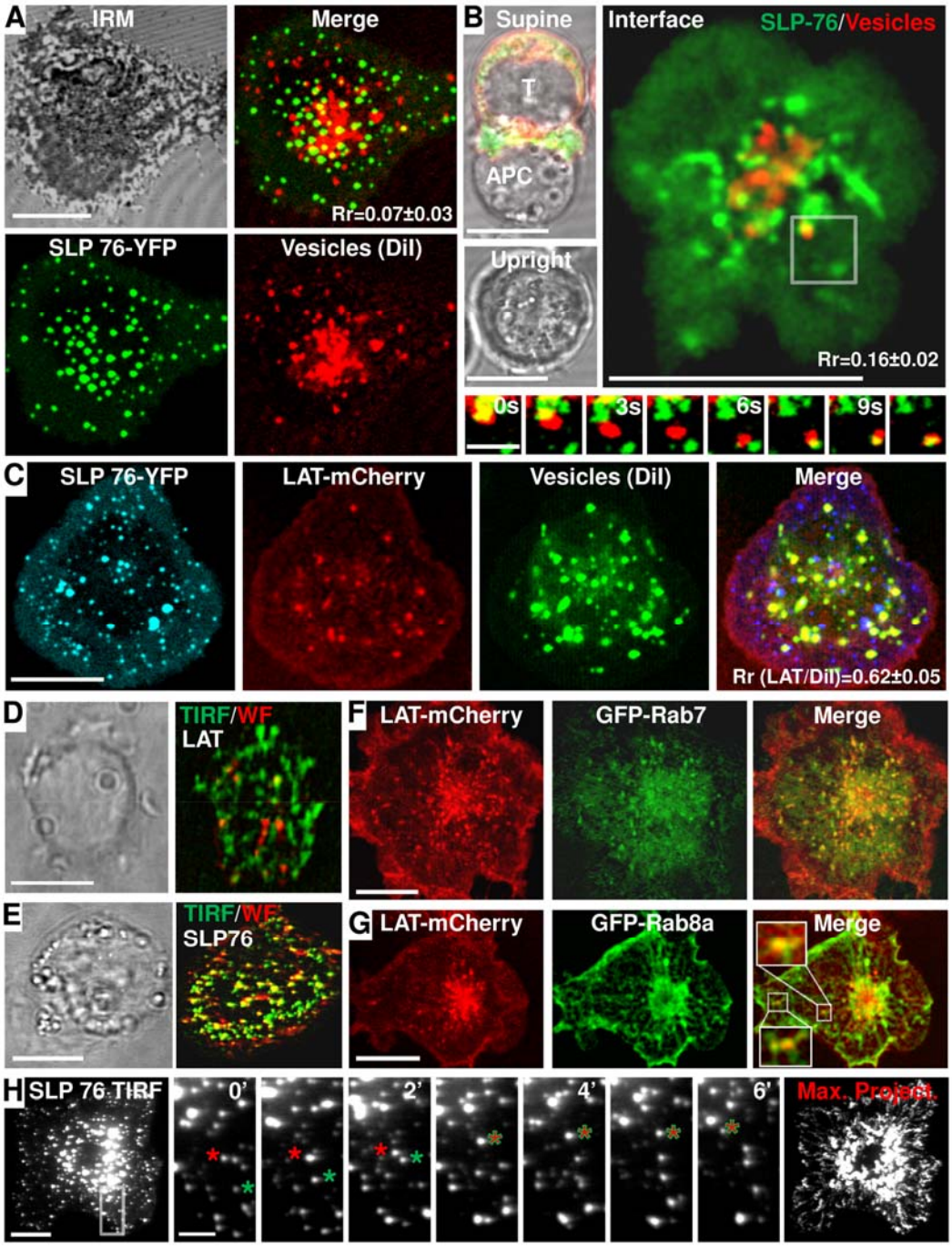
A
IRM
Merge
Rr=0.07±0.03
SLP 76-YFP
Vesicles (DiI)
B
Supine
T
APC
Upright
Interface
SLP-76/Vesicles
Rr=0.16±0.02
0s
3s
6s
9s
C
SLP 76-YFP
LAT-mCherry
Vesicles (DiI)
Merge
Rr (LAT/DiI)=0.62±0.05
D
TIRF/WF
LAT
E
TIRF/WF
SLP76
F
LAT-mCherry
GFP-Rab7
Merge
G
LAT-mCherry
GFP-Rab8a
Merge
H
SLP 76 TIRF
0'
2'
4'
6'
Max. Project.

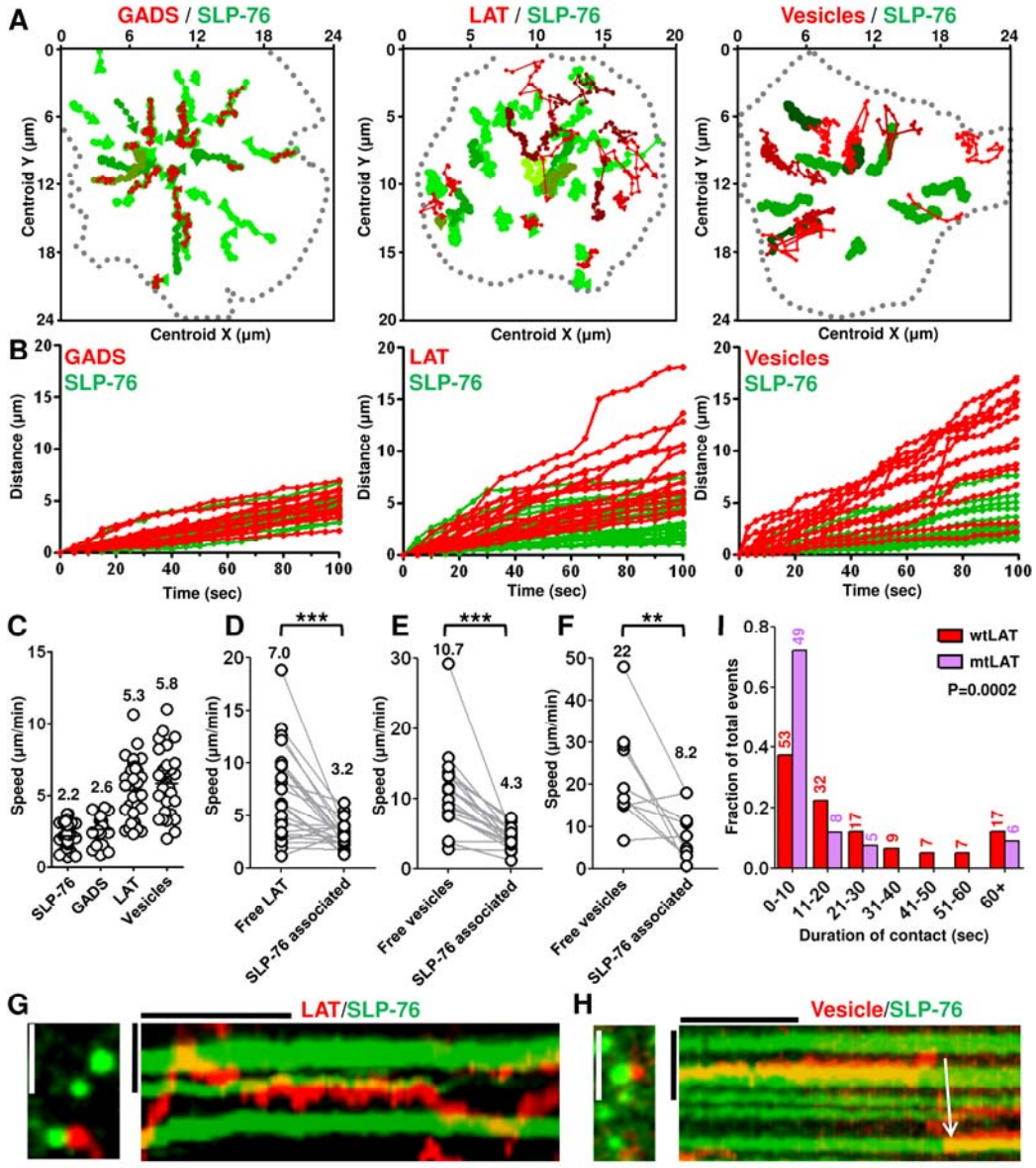
A
GADS / SLP-76
LAT / SLP-76
Vesicles / SLP-76
Centroid Y (μm)
Centroid X (μm)
B
GADS
SLP-76
LAT
SLP-76
Vesicles
SLP-76
Distance (μm)
Time (sec)
C
Speed (μm/min)
2.2
2.6
5.3
5.8
SLP-76
GADS
LAT
Vesicles
D
***
7.0
3.2
Free LAT
SLP-76 associated
E
***
10.7
4.3
Free vesicles
SLP-76 associated
F
**
22
8.2
Free vesicles
SLP-76 associated
I
wtLAT
mtLAT
P=0.0002
Fraction of total events
53
49
32
8
17
5
9
7
7
17
6
0-10
11-20
21-30
31-40
41-50
51-60
60+
Duration of contact (sec)
G
LAT/SLP-76
H
Vesicle/SLP-76

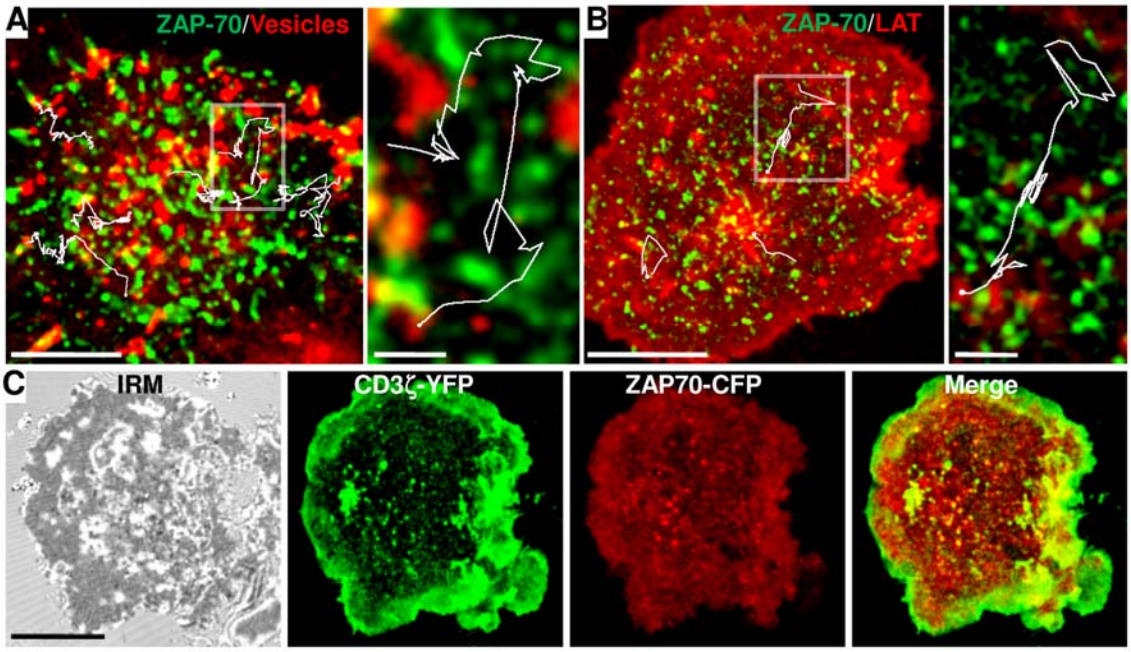
A
ZAP-70/Vesicles
B
ZAP-70/LAT
C
IRM
CD3ζ-YFP
ZAP70-CFP
Merge

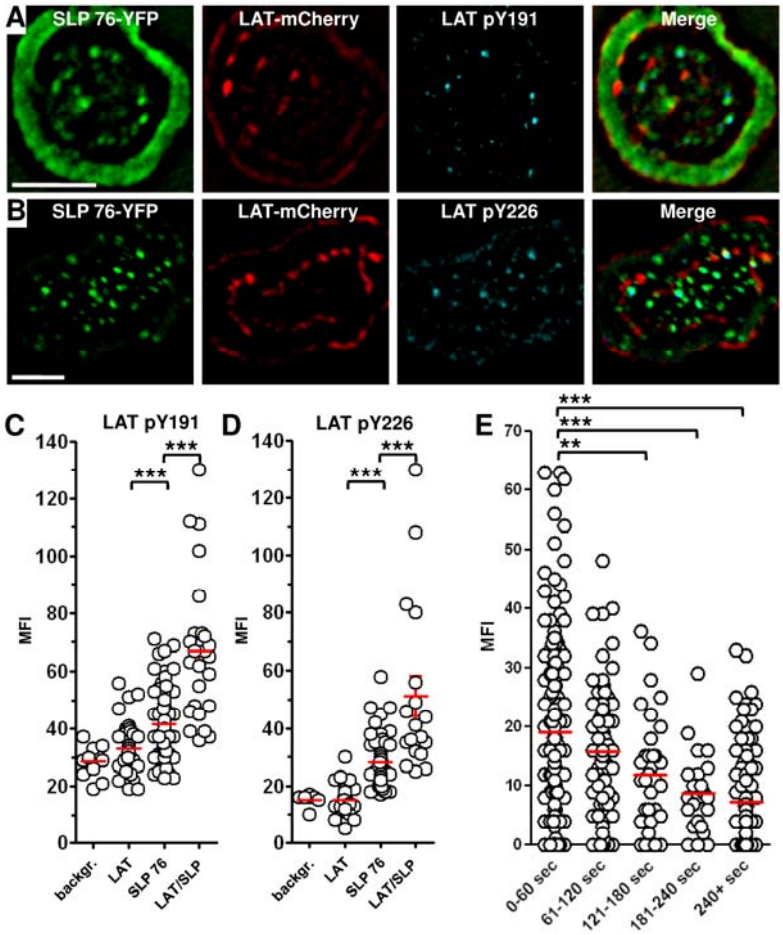
A
SLP 76-YFP
LAT-mCherry
LAT pY191
Merge
B
SLP 76-YFP
LAT-mCherry
LAT pY226
Merge
C
LAT pY191
MFI
backgr.
LAT
SLP 76
LAT/SLP
D
LAT pY226
MFI
backgr.
LAT
SLP 76
LAT/SLP
E
MFI
0-60 sec
61-120 sec
121-180 sec
181-240 sec
240+ sec

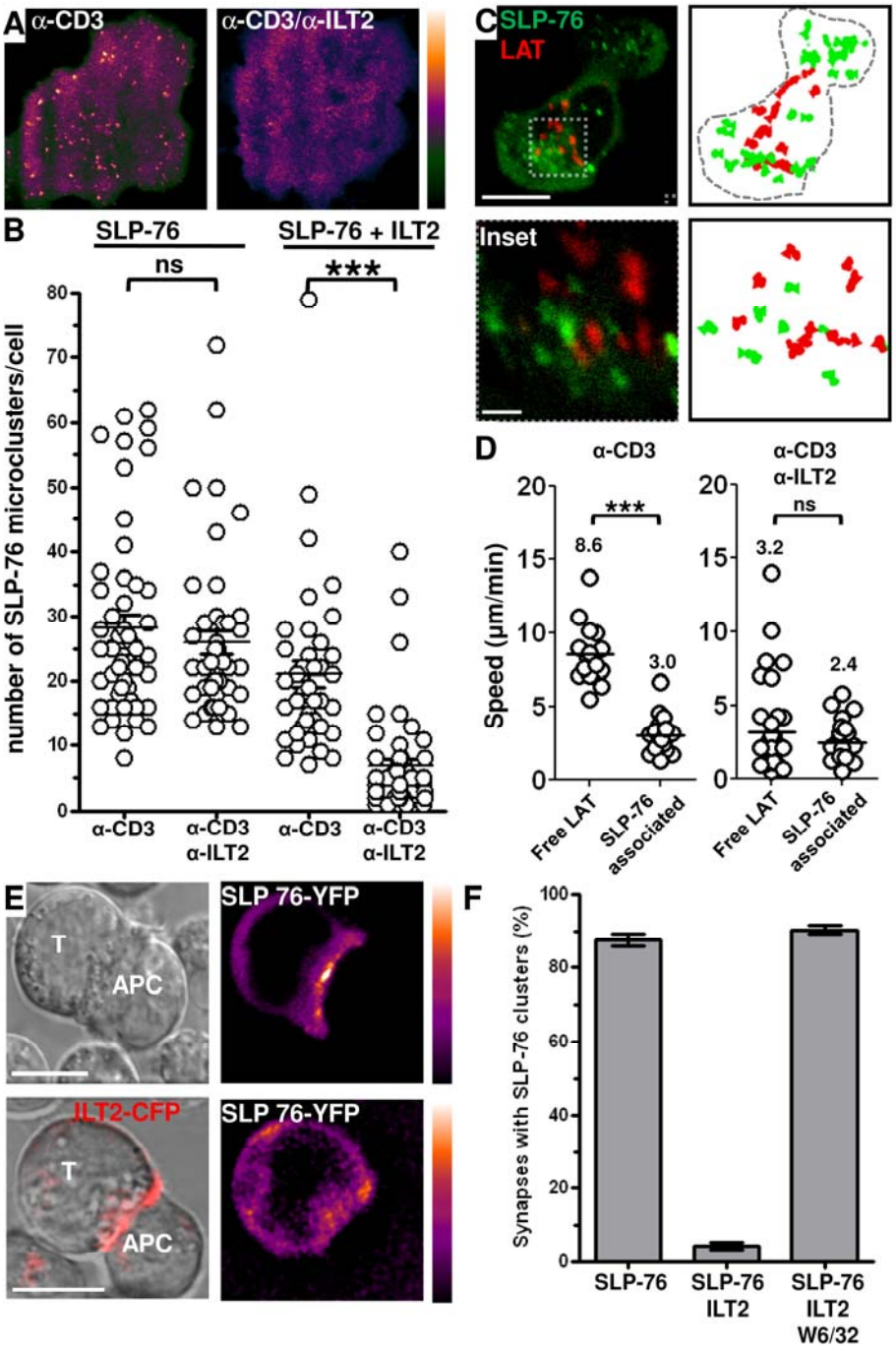
A
α-CD3
α-CD3/α-ILT2
B
SLP-76
SLP-76 + ILT2
ns
***
number of SLP-76 microclusters/cell
α-CD3
α-CD3 α-ILT2
C
SLP-76
LAT
Inset
D
α-CD3
α-CD3 α-ILT2
Speed (μm/min)
8.6
3.0
3.2
2.4
Free LAT
SLP-76 associated
E
T
APC
SLP 76-YFP
ILT2-CFP
F
Synapses with SLP-76 clusters (%)
SLP-76
SLP-76 ILT2
SLP-76 ILT2 W6/32